ACS Photonics

pubs.acs.org/journal/apchd5

Letter

Purcell Effect of Plasmonic Surface Lattice Resonances and Its Influence on Energy Transfer

Robert Collison,[⊗] Juan B. Pérez-Sánchez,[⊗] Matthew Du, Jacob Trevino, Joel Yuen-Zhou,* Stephen O'Brien,* and Vinod M. Menon*

Cite This: *ACS Photonics* 2021, 8, 2211−2219

Read Online

ACCESS | Metrics & More | Article Recommendations | Supporting Information

ABSTRACT: Engineering the density of photonic states with electromagnetic modes has become an attractive approach for controlling energy transfer between molecular systems. Here we report the use of surface lattice resonances (SLRs) that arise in arrays of metal−insulator−metal (MIM) nanocylinders to control the energy transfer between two archetypal molecular dyes, P580 (donor) and P650 (acceptor). When the SLR is detuned from the donor emission, energy transfer is observed as expected, with donor emission decreasing with respect to the acceptor emission (donor/acceptor peak fluorescence ratio = 0.45). In contrast, when the SLR is tuned to the donor emission, Purcell enhancement becomes dominant, outcompeting energy transfer and suppressing acceptor emission (donor/acceptor peak fluorescence ratio = ∼5.4). To analyze these observations, a kinetic model was developed, based on pumping rate, donor-to-acceptor energy transfer rate, and radiative and nonradiative decay of the dyes. The results suggest the additional decay channel introduced by the SLR for which $\lambda^{\mathrm{SLR}}_{k_{\parallel}=0} = \lambda^{\mathrm{donor}}_{\mathrm{emission}}$ competes strongly with the energy transfer process, while SLRs that coincide with donor emission peaks at larger values of in-plane momentum $k_{\parallel}$ have a less pronounced effect. Our study highlights the wide range of SLR-based Purcell effects possible by simple changes in the lattice dimensions and their consequences in the kinetics of molecular energy transfer processes in the condensed phase.

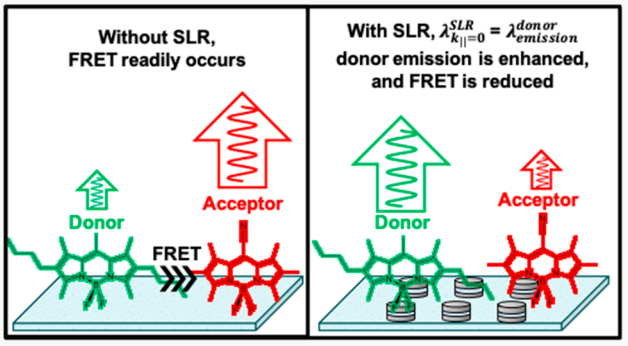

KEYWORDS: *aluminum, plasmons, BODIPY, surface lattice resonances, Rayleigh anomalies, diffraction gratings, Förster resonant energy transfer*

When plasmonic nanoparticles with localized surface plasmon resonances (LSPRs) are arranged in two-dimensional (2D) lattices, the in-plane scattering fields of the individual particles mutually interfere to form extended modes known as surface lattice resonances (SLRs). Many studies have demonstrated the utility of SLRs for producing narrow, high-Q optical resonances with controllable line widths and dispersions determined by the lattice geometry and nanoparticle diameter.[1−6]

Just as the excitons of dye molecules and quantum dots (QDs) can couple to the resonant modes of optical microcavities, molecular and semiconductor excitons can couple to SLRs when dye molecules or QDs are in the plane of the plasmonic lattice. Several studies suggest coupling the highly localized Frenkel excitons of organic molecules or inorganic semiconductor QDs to laterally extended SLRs can "delocalize" the excitons and increase their diffusion lengths.[7−9] While extending the diffusion length is of interest for photovoltaic applications, another important use of SLRs is in modifying the light emission from molecular and quantum dot emitters.[10] Here the collective resonances have been exploited to enhance the overall quantum efficiency of the emitters. In this work, we address the interplay between the changes in diffusion through coupling to SLRs and the overall modification in exciton lifetime by studying Förster resonant energy transfer (FRET) between a donor−acceptor pair under weak coupling to SLRs.

FRET, the transfer of excitation from one molecule to another by dipole−dipole interactions over short distances (usually within 10 nm) is a major contributor to exciton diffusion.[11−14] In some studies of organic semiconductor films and crystals, the equations that describe FRET were used to model exciton diffusion.[15,16] Previously, the diffusion length, L_{diff}, of singlet excitons in crystalline films of small molecule

Received: April 22, 2021
Published: August 5, 2021

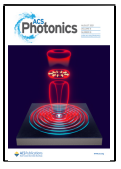

dyes has been approximated based on the experimentally measured FRET radius, R_0 (i.e., the homo-FRET or self-transfer radius) using the simple expression $L_{diff} = \frac{1}{\sqrt{6}}\frac{R_0^3}{b^2}$, where b is the lattice constant of the dye molecules in the film, assuming a simple cubic lattice.[17] Based on these approximations, it is reasonable to treat FRET between two different dyes as a proxy for exciton diffusion. Specifically, one might reasonably expect that SLR−exciton coupling that enhances or inhibits FRET would likewise enhance or inhibit exciton diffusion, at least as far as singlet excitons are concerned.

Multiple studies have also shown that various confined photonic modes, specifically photonic crystal resonances,[18] microcavity photonic modes,[19−22] localized surface plasmons,[23] surface plasmon polaritons,[24,25] and plasmonic waveguides[26] can enhance energy transfer from a donor dye to lower-energy acceptor dye, resulting in the transfer of energy over distances greater than those permitted by unenhanced Dexter (≤1 nm) and Förster resonant energy transfer (≤10 nm). In many of these reports, such as the reports of enhanced energy transfer between small-molecule dyes and *J*-aggregates of cyanine dyes, the donor exciton is strongly coupled to the resonant modes of the microcavity, and in some cases, both the donor and the acceptor excitons are coupled to a single cavity mode to generate multiple polariton modes.[19,20] The strong coupling component could be an essential feature for increasing the FRET rate.

Meanwhile, there are conflicting reports on whether the FRET rate is directly affected by the local density of optical states (LDOS). It is well-known that, compared to emitters in free space, emitters coupled to microcavities and other photonic structures exhibit different rates of radiative decay and that these increased or decreased rates of emission correspond to the greater or lesser LDOS of the photonic structure compared to free space, well-known as the Purcell effect.[27,28] While the Purcell effect for visible light emitters and photonic structures is well-known, there is still debate as to whether increasing LDOS is sufficient to increase the rate of FRET. One seminal report found that both the rate of fluorescence from a donor dye and the rate of FRET from this donor to an acceptor were linearly related to each other, and that they both varied when the LDOS was varied by placing the dyes layers in microcavities of various thicknesses.[29] A recent report likewise found that the rate of FRET between two dyes increases linearly with LDOS.[30] However, a set of theoretical and experimental studies found that using nanophotonic structures to alter the LDOS could increase or decrease FRET efficiency but cannot affect FRET rates when the dyes were in dispersionless dielectric enviornments.[31−34]

Within the weak coupling regime, due to the Purcell enhancement, it is conceivable that modifying LDOS may not modify the FRET rate, although it may modify the FRET efficiency by changing the rates of competing excited donor decay processes (emission and nonradiative decay channels). In addition to changes in the LDOS, formation of a polariton or splitting of the exciton band, as occurs in the strong coupling regime, may also alter the FRET rate. Considering these conflicting experimental and theoretical results on the topic of photonic modes, LDOS, and FRET rates and efficiencies, it is important to consider how coupling of donor molecules to the SLR influences energy transfer. The central question is if the modification in the excited state lifetime of the donor through coupling to the SLRs alters the FRET rate and FRET efficiency.

EXPERIMENTAL RESULTS AND DISCUSSION

Given the potential for SLRs to delocalize organic excitons in the lattice plane and the demonstrated capacity of various low-dimensional photonic and plasmonic modes to increase the rate and efficiency of energy transfer between dyes, we could expect that coupling a donor dye to a SLR would increase the rate of energy transfer between the donor and an acceptor when the two are blended together in a film covering the SLR-supporting lattice.[25] However, this phenomenon was predicted under the strong coupling of donor transitions to the confined electromagnetic mode, with the concomitant formation of polariton states.[25] In the present study, under the weak coupling regime, which has been less studied, we find the exact opposite: the FRET rate is found to be suppressed because of the competition between the change in the excited state lifetime by the SLR versus the delocalization provided by the SLR mode. We found this effect to be especially dominant when the donor emission overlaps with the SLR mode at $k_{||} = 0$. Specifically, this SLR promoted emission and nonradiative decay from the excited donor dye molecules and inhibited energy transfer to the acceptor.

The SLR-supporting lattices used in these experiments were square lattices of vertically layered Al−Al_2O_3−Al (Al-MIM for Al−metal−insulator−metal) nanocylinders. These lattices were fabricated onto a glass substrate using electron beam lithography (EBL). A film containing 800 mM (20 wt %) of the donor dye (P580) and 8 mM (0.16 wt %) of the acceptor (P650) dispersed in poly(methyl methacrylate) (PMMA) was spin-coated onto the glass substrate and SLR-supporting lattices, and the film's fluorescence spectra on the bare substrate and on the lattices were studied. The fabrication and spectroscopic procedures are described in Methods, and optical microscope images, scanning electron microscope (SEM) images, and dimensional diagrams of the lattices are shown in Figure 1.

The choice of Al as the plasmonic material in these lattices was made to produce lattices that were stable in air and support SLRs across the visible range of wavelengths. Multiple reports show that Al nanoparticles can support LSPRs[35−37] and SLRs[4,38,39] across the visible range and into the ultraviolet. In contrast, Au nanoparticles, frequently used for SLRs, generally cannot support resonances for λ < 500 nm due to the onset of interband absorption, and the minimum attainable LSPR wavelength for Au particles is even longer for Au particles with Ti or Cr adhesion layers than for pure Au particles.[40−43]

Furthermore, although Ag nanoparticles can support LSPRs and SLRs across the visible range, they tend to oxidize unless coated with an inert dielectric, such as Al_2O_3. In contrast, Al nanoparticles spontaneously form an approximately 3 nm thick layer of Al_2O_3 upon exposure to the atmosphere that prevents further oxidation, preserving the plasmonic properties of the underlying nanostructures.[35] The choice to use MIM nanocylinders rather than simple Al disks was inspired by reports of SLR lattices made of Ag- and Al-MIM nanostructures[44−46] and by the assumption that MIM nanocylinders featuring two 50 nm thick Al disks would exhibit a greater scattering cross section than simple 50 nm thick Al disks.

Following the same strategy as previous work,[47] the Al-MIM nanocylinder lattices had various lattice constants (α) to

https://doi.org/10.1021/acsphotonics.1c00616
ACS Photonics 2021, 8, 2211−2219

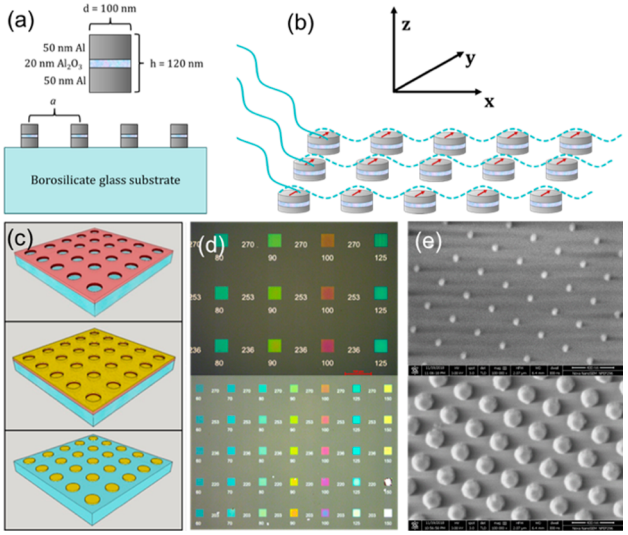

Figure 1. Images of Al-MIM lattices showing nanocylinder dimensions, fabrication process, and brightfield microscope images. (a) Illustration (front view) of a square lattice of Al-MIM nanocylinders on a glass substrate showing the variable lattice constant, a, and the dimensions of the Al-MIM nanocylinders, which are the same in all four lattices that were used for energy transfer experiments. (b) Illustration of the excitation of an SLR in the nanocylinder array, with axes labeled. The x and y axes are the axes of the square lattices of nanocylinders, the z axis is the axis perpendicular to the plane of the lattices, and the plane of incidence for the transmitted light is the xz-plane (as determined by the orientation of the entry slit to the spectrometer). The coherent, in-phase excitation of the dipolar LSPRs of the Al-MIM nanocylinders (red arrows) by s-polarized light is illustrated. For s-polarized light, the electric field of the incident light and the electric dipoles of the nanocylinders are oriented parallel to the y-axis, and the SLRs excited by s-polarized light propagate along the x-axis. (c) Depiction of the fabrication process, consisting of three basic steps, EBL to produce a lattice of holes in the PMMA film (top), followed by metal deposition (middle) and lift-off in warm acetone (bottom). (d) Two bright-field optical microscope images (20× magnification for upper image, 10× for lower) of the finished arrays of Al-MIM pillars. Each square patch of particles is 50 μm × 50 μm in area. (e) Scanning electron microscope (SEM) micrographs of Al-MIM nanocylinder lattices. The scale bars in the lower right corner of both SEM micrographs in (e) are 400 nm long.

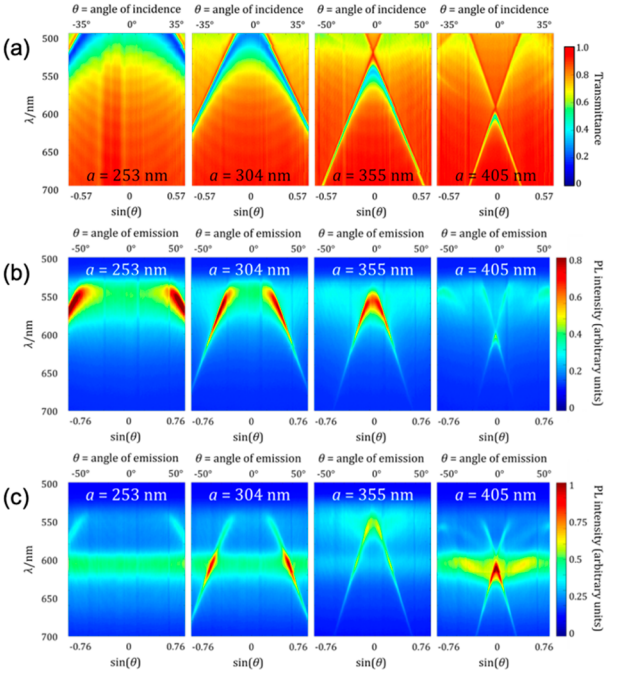

Figure 2. Angle-resolved spectra showing dispersions of SLRs for various lattices without dye, with donor dye, and with donor and acceptor dye. (a) Angle-resolved transmission spectra of lattices of Al-MIM nanocylinders on glass, s-polarized light. The lattice constant, a, varied from 253 to 405 nm, as indicated on the spectra. They very clearly show the s-polarized (±1, 0) SLRs (the blue curved features), which result in a sharp decrease in transmission of light due to a combination of light absorption and reflection at wavelengths slightly longer than the corresponding (±1, 0) Rayleigh Anomalies (RAs). The RAs themselves appear as the red or orange X-shaped features, representing local peaks in transmission. (b) Angle-resolved s-polarized fluorescence spectra of the same lattices of Al-MIM nanocylinders as in (a) coated in 400 mM P580 (donor dye) in PMMA. (c) Angle-resolved fluorescence spectra of the same lattices, this time coated in a nm film containing 800 mM P580 (donor) and 8 mM P650 (acceptor) in PMMA. Note that no polarizing filters were used for collected fluorescence. As a result, the spectra in (c) show light coupled to both the s-polarized (±1, 0) and the p-polarized (0, ±1) SLRs.

differentiate between photonic effects of individual NPs (LSPRs) and supported SLRs, which spanned the range of wavelengths in which the dyes absorb and emit. Specifically, the Al-MIM nanocylinder lattices having lattice constants a = 253, 304, 355, and 405 nm produced SLR modes whose peak extinction wavelengths at $k_{\|}$ = 0 ($\lambda^{SLR}_{k_{\|}=0}$) were 462, 502, 551, and 615 nm, respectively. These values for $\lambda^{SLR}_{k_{\|}=0}$ were determined experimentally by measuring the angle-resolved transmission spectra of the lattices without any dyes (Figure 2a). For the following discussion of these lattices and their spectra, the plane containing the Al-MIM lattice is referred to as the xy-plane, and the optical plane of incidence with which the angle-resolved spectra were measured is the xz-plane (see the cartoon in Figure 1b). Under these designations, k_y = 0 and $k_{\|} = k_x$, as in eq 1:

$$k_{\|} = k_x = \frac{2\pi(\text{radians}) \times \sin(\theta)}{\lambda} \quad (1)$$

To assess the influence of the SLRs on the energy transfer between the boron dipyrromethene (BODIPY) dyes, the two dyes were dissolved in a solution of poly(methyl methacrylate) (PMMA) in anisole and spin-coated onto a glass substrate in a film containing 800 mM (20 wt %) of the donor dye and 8 mM (0.16 wt %) of the acceptor dye in solid PMMA. These concentrations were selected so that both dyes would exhibit measurable fluorescence intensities. Specifically, larger concentrations of acceptor tended to reduce the intensity of the donor dye's fluorescence to near background levels. By using a 100:1 concentration ratio, the acceptor serves as a probe for the effects of coupling between the SLR and donor, without quenching or absorbing the donor's fluorescence entirely (at least for the control sample, i.e., the donor−acceptor−polymer film on the glass substrate).

Additionally, the high concentration of the donor dye in the donor−acceptor−PMMA film was used to maximize the strength of the coupling between the donor excitons and the SLRs, given that the degree of strong coupling is proportional to $\sqrt{(N/V)}$, where N is the number of coupled dye molecules and V is the mode volume of the photonic resonance.[48]

https://doi.org/10.1021/acsphotonics.1c00616
ACS Photonics 2021, 8, 2211−2219

However, we did not observe evidence of strong coupling between the donor (or acceptor) dye and the SLRs in our samples, and the changes in FRET efficiency and donor emissivity that we observed are explained by weak coupling and the Purcell effect.

Table 1 shows the absolute peak fluorescence intensities in counts per second (cps) for the donor (I'_D) and acceptor (I'_A) dyes from a blended film on Al-MIM lattices with various lattice constants, their ratio, and the approximated FRET efficiency measured on the glass substrate and each SLR-supporting lattice.

Table 1. Estimated Energy Transfer Efficiencies for the Donor−Acceptor−Polymer Film on Different SLR-Supporting Lattices

Al-MIM lattice	$\lambda^{SLR}_{k_\parallel=0}$ (nm)	$I'_D/10^5$ cps	$I'_A/10^5$ cps	(I'_D/I'_A)	η^*[a] (%)
glass substrate		NA[b]	NA[b]	0.45	79
α = 253 nm	462	6.68	10.7	0.63	73
α = 304 nm	502	6.94	11.4	0.61	73
α = 355 nm	551	10.3	1.91	5.4	24
α = 405 nm	615	5.52	14.5	0.38	81

[a]Here, η^* are estimates of the FRET efficiency See the Supporting Information (SI) for details. [b]Due to a change in instrument parameters during measurement, the absolute fluorescence intensities of the donor−acceptor−polymer film on the bare glass substrate are not directly comparable to the absolute intensities from the lattices. As such, the intensities pertaining to the blended film on the bare glass substrate (1.64×10^4 cps and 4.60×10^4 cps for donor and acceptor, respectively) are omitted from this table to avoid misleading the reader into thinking that they are directly comparable to the lattice intensities. This change does not affect the shape of the measured film-on-glass fluorescence spectrum.

Spectroscopy of the Al-MIM Lattices and BODIPY Dyes. On the bare glass substrate, in the absence of any Al-MIM structures, the acceptor's fluorescence peak intensity at 609 nm, I'_A, exceeded the donor's peak fluorescence intensity at 550 nm, I'_D, giving a ratio, I'_D/I'_A, of 0.45, indicating that energy transfer from donor to acceptor is occurring. When the same film was coated onto the SLR-supporting Al-MIM lattices, the values of I'_D, I'_A, and their ratio varied according to the extent to which the SLR at $k_\parallel$ = 0 overlapped with the donor's fluorescence peak at 550 nm. The lattices having $\lambda^{SLR}_{k_\parallel=0}$ 462 and 502 nm marginally increased the I'_D/I'_A ratio from 0.45 to 0.63 and 0.61, respectively, and the lattice with $\lambda^{SLR}_{k_\parallel=0}$ = 615 nm decreased the I'_D/I'_A ratio slightly from 0.45 to 0.38 due to an increase in the radiative decay rate of the acceptor, γ^r_A, on this lattice (Table 2). In contrast, the lattice with $\lambda^{SLR}_{k_\parallel=0}$ = 551 nm drastically increased the I'_D/I'_A ratio to 5.4, such that the emission from the donor dye exceeded that of the acceptor. This difference in the fluorescence spectrum of the donor−acceptor−PMMA film when it is coupled to the 551 nm SLR compared to the other SLRs is apparent in the angle-resolved fluorescence spectra shown in Figure 2c and in the angle-integrated fluorescence spectra in Figure 3.

Table 2. Energy Transfer Rates (K_E), Radiative ($\gamma^r_{D,A}$) Decay Rates in ns^{-1}, and Relative Steady State Populations ($N^{(ss)}_D/N^{(ss)}_A$) for the Donor−Acceptor−Polymer Film on Different Lattices

Al-MIM lattice	$\lambda^{SLR}_{k_\parallel=0}$ (nm)	K_E	γ^r_D	γ^r_A	$N^{(ss)}_D/N^{(ss)}_A$
glass substrate		0.169	0.069	0.051	0.309
α = 253 nm	462	0.169	0.181	0.096	0.585
α = 304 nm	502	0.169	0.183	0.087	0.536
α = 355 nm	551	0.169	0.307	0.080	0.496
α = 405 nm	615	0.169	0.121	0.112	0.679

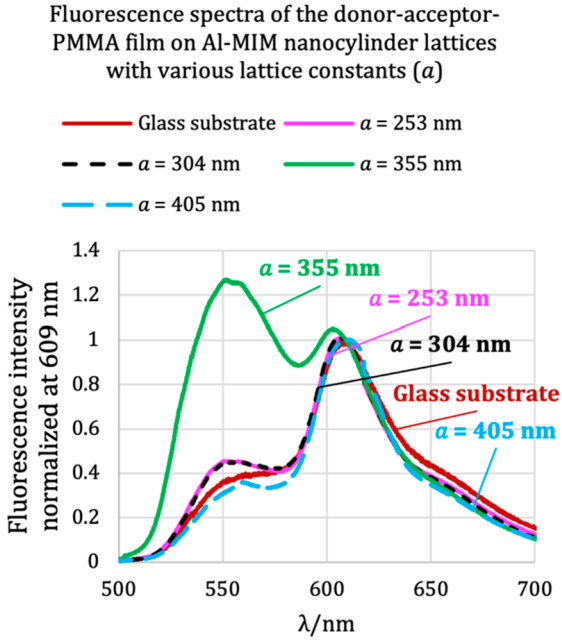

Figure 3. Fluorescence spectra of the blended donor and acceptor film coated onto various Al-MIM lattices, integrated over all angles of incidence collected by the objective lens (−53° to 53° relative to the surface normal). The spectra are normalized at the acceptor's emission peak at 609 nm to show the change in the shape of the donor−acceptor−-polymer film's fluorescence spectrum when the film is coated on various Al-MIM lattices. Note that the abrupt decrease in intensity at 620 nm in the α = 304 and 405 nm spectra is due to bleaching of the sample that creates a stitching error in the step-and-glue function of the spectrometer. Fortunately, this error did not affect the 550 or 609 nm fluorescence intensities that were used as the indicative wavelengths for the donor and acceptor dyes, since these were captured in the same frame.

Furthermore, the absolute intensities of the donor and acceptor dye fluorescence peaks in Table 1 show that the $\lambda^{SLR}_{k_\parallel=0}$ = 551 nm SLR increased I'_D/I'_A by both increasing I'_D and decreasing I'_A compared to the other SLRs. The observation that the maximum I'_D and minimum I'_A values measured occur together for the $\lambda^{SLR}_{k_\parallel=0}$ = 551 nm SLR suggests that the SLR that is resonant with the donor's fluorescence peak at $k_\parallel$ = 0 enhances emission of the donor at the expense of energy transfer to the acceptor. One explanation is that the $\lambda^{SLR}_{k_\parallel=0}$ = 551 nm SLR provides a channel for the accelerated radiative and nonradiative decay of the excited donor dyes, such that the total decay rate of the donor exceeds the FRET rate. Enhancement of nonradiative decay of exited donor molecules cannot account for the increase in the donor dye's fluorescence, but in our model it contributes to the decrease in energy transfer that is observed with the $\lambda^{SLR}_{k_\parallel=0}$ = 551 nm SLR compared to the other SLRs and the bare glass substrate. Additional experiments, such as conductivity and photocurrent

https://doi.org/10.1021/acsphotonics.1c00616
ACS Photonics 2021, 8, 2211−2219

measurements, would be required to measure the effect of exciton−SLR coupling on nonradiative decay experimentally.

Notably, the SLRs having $\lambda^{SLR}_{k_{||}=0}$ = 462 and 502 nm did not inhibit energy transfer, as the $\lambda^{SLR}_{k_{||}=0}$ = 551 nm SLR did, even though these SLRs overlapped significantly with the donor emission peak at larger values of $k_{||}$ (at angles of emission of 20° and 50°). This discrepancy suggests that coupling the donor emission to an SLR at $k_{||}$ = 0 specifically (that is, at 0° angle of emission) is effective for promoting radiative decay of the donor dye into free space, whereas coupling the donor emission to SLRs at other values of $k_{||}$ may be less effective for outcoupling the donor dye's fluorescence. Furthermore, coupling the donor exciton (that is, the donor absorption peak at 518 nm) to SLRs at $k_{||} > 0$, shown in Figure 2b for the $\lambda^{SLR}_{k_{||}=0}$ = 462 and 502 nm SLRs did not increase energy transfer as expected.

Meanwhile, the $\lambda^{SLR}_{k_{||}=0}$ = 615 nm SLR, which approximately coincides with the acceptor's fluorescence peak at 609 nm, maximized I'_A and minimized I'_D compared to the other SLRs (Table 1). This observation suggests that the $\lambda^{SLR}_{k_{||}=0}$ = 615 nm SLR may have enhanced the energy transfer process. However, it is not clear that a significant enhancement of energy transfer occurred, since the decrease in I'_D/I'_A compared to the same film on bare glass is marginal, and the absolute intensity of the donor is only slightly lower for this SLR than for the other nondonor-resonant SLRs at 462 and 502 nm. The enhancement of I'_A compared to the other SLRs, while significant, could be mostly due to enhancement of the fluorescence of the dyes rather than an increase in the rate of energy transfer.

COMPUTATIONAL MODELING

To model the donor−acceptor energy transfer kinetics in the SLR nanostructure, we consider a nanoparticle (NPs) lattice as a 1D chain of dipolar entities. We calculate the total Purcell factors for the emitters in the nanostructure using classical electromagnetism.[49,50] Finally, we incorporate the corresponding decay rates in a kinetic model to explain the emission spectra at steady state conditions.

In our kinetic model, where P, K_E, and $\gamma^T_{D/A} = \gamma^r_{D/A} + \gamma^{nr}_{D/A}$, correspond the rates of pumping, donor-to-acceptor energy transfer, and radiative decay, and total (as a sum of radiative and nonradiative contributions) decay of the dyes, respectively. The corresponding equations are described in detail in the SI (eqs S1−S20). For simplicity, we consider the dyes to be halfway between two nanoparticles. Under these circumstances, where the dyes are well-separated from the nanoparticles (>50 nm), the Purcell factor corresponds mostly to the enhancement of radiative decay[51] ($\gamma^T_{D/A} \approx \gamma^r_{D/A} > > \gamma^{nr}_{D/A}$). This Purcell enhancement slowly decreases as the emitter is moved toward one of the NPs and decreases even faster as it is moved out of the plane of the lattice. Table 2 summarizes the calculated energy transfer and decay rates for the donor and acceptor dyes on the bare glass substrate and on the Al-MIM lattices.

The results in Table 2 are a direct consequence of the Purcell factor profiles in Figure 4. First, it needs to be clarified that, under steady state conditions, a higher emission intensity from the donors does not necessarily imply a higher relative concentration of excitations in the donors, and analogously for acceptors. According to our calculations, the altered LDOS due to the plasmonic lattice changes the relative emission

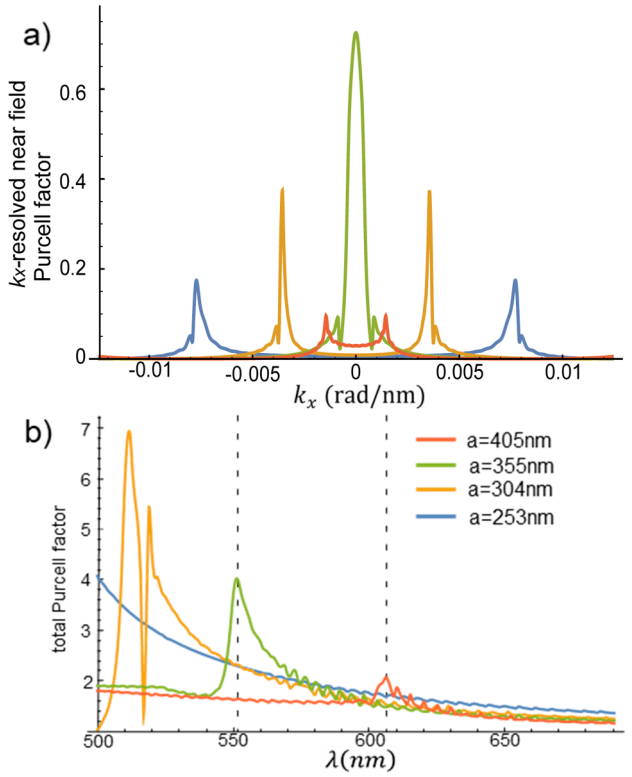

Figure 4. Purcell factor F for different lattice constants. (a) Near-field k_x-resolved Purcell enhancement, defined as $\frac{6\pi\epsilon_0 n_2^2}{|\boldsymbol{\mu}|^2 k(\lambda)^3}\mathrm{Im}(\boldsymbol{\mu}^* \cdot \vec{\mathbf{G}}_{self}(\lambda, k_x) \cdot \boldsymbol{\mu})$, showing the contribution of a k_x lattice mode to the Purcell enhancement at λ = 551 nm. (b) Total Purcell factor obtained by adding far-field and near-field contributions, the latter being integrated over the first Brillouin zone $\left[-\frac{\pi}{a}, \frac{\pi}{a}\right]$. We assume the emitters are located halfway between two NPs in the middle of the lattice. See eqs S17 and S18 in the Supporting Information for more details.

intensities of donors and acceptors, but it does not affect the donor-to-acceptor energy transfer rate K_E. This is expected for the dye molecules in the dye-doped PMMA films that are relatively far away (over 10 nm) from the NPs.[52] A more detailed analysis showed that the energy transfer rate K_E can indeed be modified when the separation between the dyes is comparable with the distance between them and the NPs. We suspect having a lower concentration of dyes would allow us to have more control over the energy transfer kinetics by directly modifying K_E.

The steady state population of donor excitations relative to that of acceptors is $N^{(ss)}_D/N^{(ss)}_A = \gamma^T_A/K_E$ (see SI). This ratio is independent of any competition between the decay channel γ^T_D and the energy transfer channel K_E, as the latter only affects the absolute donor and acceptor populations. Given that K_E is not affected by the NP lattice, changes in the donor/acceptor population ratio in the plasmonic lattice depend only on the decay rate of the acceptor γ^T_A. For the SLRs at $\lambda^{SLR}_{k_{||}=0}$ = 615 nm, the very fast decay of the acceptors decreases their steady state population significantly, such that most excitations in the system are in the donors. This effect might seem counterintuitive given that, for such a lattice (a = 405 nm), we observe a higher emission at the acceptor's emission wavelength; however, there is no inconsistency, as we shall explain below.

https://doi.org/10.1021/acsphotonics.1c00616
ACS Photonics 2021, 8, 2211−2219

The power emitted by the donors relative to that of acceptors $I'_D/I'_A \approx \gamma^r_D N^{(ss)}_D/\gamma^r_A N^{(ss)}_A \approx \gamma^T_D/K_E$ does indeed depend on the competition between the decay channel γ^T_D and the energy transfer channel K_E. The emission intensities vary almost linearly with the total decay of the donor. Notice how for $\lambda^{SLR}_{k_\parallel=0}$ = 462 and 502 nm SLRs, we have $\gamma^T_D < K_E$, which implies that donor-to-acceptor energy transfer dominates the kinetics, and the emission intensity from the acceptors exceeds the emission from the donors. For the SLRs at $\lambda^{SLR}_{k_\parallel=0}$ = 551 nm, the Purcell factor of the donor is higher than for any other lattice, making $\gamma^T_D > K_E$ and yielding the highest ratio I'_D/I'_A. Interestingly, for the SLRs at $\lambda^{SLR}_{k_\parallel=0}$ = 615 nm, the Purcell factor of the donor is the lowest and so is the ratio I'_D/I'_A. The latter suggests that the relatively high acceptor emission for the lattice a = 405 nm is not due to a Purcell factor of the acceptors, but to a relatively slow decay of donors for this lattice.

The results obtained using the 1D lattice provide a semiquantitative description of the results found in the experiment. The main factors that prevent us from having a quantitative comparison with the experiment include the lack of calculation of nonradiative decay rates for the emitters $\gamma^{nr}_{D/A}$, the geometric effects of individual NPs, and orientational averaging, as well as a 1D model. Furthermore, the calculations account for the total emission, while the experiment only measures the emission in a certain angle window θ = [−50°, 50°] (see, also, Figure 5).

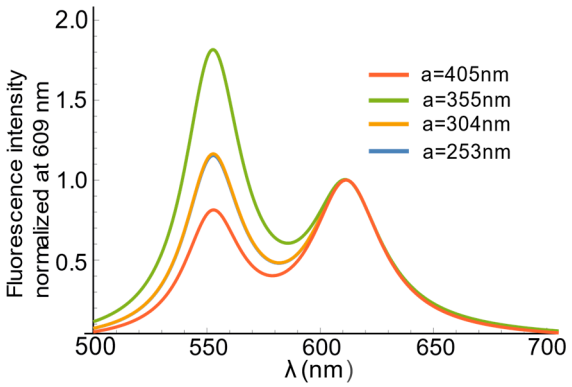

Figure 5. Theoretical normalized emission spectra for the lattice constants used in the experiment.

CONCLUSIONS

Based on the fluorescence spectra of the donor−acceptor−polymer film coated onto the glass substrate and various SLR-supporting Al-MIM lattices, we found that the lattice supporting the SLR that overlapped the most with the donor dye's fluorescence peak at $k_\parallel$ = 0 inhibited energy transfer compared to the bare glass substrate and the other SLR-supporting lattices and also maximized the donor dye's fluorescence and minimized the acceptor's fluorescence compared to the other lattices. Taken together, these observations indicate that the SLR that is resonant with the donor dye's fluorescence peak at $k_\parallel$ = 0 promotes the radiative decay of the donor, increasing the portion of excited donor dye molecules that emit into free space and decreasing the portion that transfers their exciton energy to acceptor dye molecules. The net result is more emission from the donor dye and less emission from the acceptor. Future experiments may need to use conductance and photocurrent measurements to measure the nonradiative decay of excitons and to assess how exciton−SLR coupling influences those decay channels.

Interestingly, the two SLRs that were resonant with the donor emission peak at higher values of $k_\parallel$ and oblique angles of incidence (20° and 50°, respectively) only marginally inhibited energy transfer, indicating that the overlap of the SLR and the donor dye's fluorescence peak specifically at $k_\parallel$ = 0 and a 0° angle of emission, normal to the lattice plane, appears to be a key factor in enhancing the radiative and nonradiative decay of the donor and avoiding energy transfer. The donor−acceptor pair used here exhibits very efficient energy transfer in the absence of SLRs, at least when they are combined in the concentrations we used in a PMMA film. It is likely that, as predicted in a previous study,[25] donor−SLR strong coupling might enhance FRET, especially if the lattice and dye are matched such that the SLR is tuned to the donor dye's exciton (to its peak absorption wavelength) at $k_\parallel$ = 0 instead of coupling to the dye's emission peak at $k_\parallel$ = 0. For those experiments, it might be better to use modes having a normal dispersion (as opposed to an anomalous dispersion). SLRs having a normal dispersion, in which the resonant frequency of the SLR is at a minimum at $k_\parallel$ = 0, can obtained with the quadrupole-like resonances of elongated or rectangular nanoparticles,[6] and this effect could be more easily observed obtained using dyes that do not undergo FRET in the absence of photonic mode coupling, as in Zhong et al.[19]

Energy transfer can enhance certain devices, such as solar cells,[15,53−58] light-emitting diodes (LEDs),[59] and photocatalysts.[60] Nevertheless, the inhibition of energy transfer could be equally useful. FRET inhibition could promote emission from a higher-energy fluorophore, while inhibiting undesirable energy transfer to a lower-energy exciton trap, such as in an organic LEDs in which energy transfer to impurities in the phosphor or host material undermines the device's brightness, efficiency, or color purity. The results of this study indicate that SLRs might be suitable for enhancing organic or quantum dot LEDs by increasing outcoupling of fluorescence from an organic or quantum dot phosphor, even when impurities or surface defects in the phosphor or host material that would otherwise function as exciton traps are present. This effect could even be used to dynamically modulate energy transfer in a system in which the wavelengths at which the SLR occurs can be changed in real time by altering the lattice constant using a stretchable substrate[61] or by changing the refractive index of the dielectric surrounding the plasmonic particles.[62]

METHODS

Fabrication of Al-MIM Nanocylinder Lattices. Square lattices of Al-MIM nanocylinders were fabricated by EBL using PMMA as the resist, followed by Al and Al_2O_3 deposition using electron beam evaporation and, finally, lift-off in warm acetone. To allow the fabrication of relatively tall structures (100 nm diameter nanocylinders, 120 nm total height), a PMMA bilayer was used to ensure good lift-off. The experimental details of this fabrication method are described in the SI.

Application of Dye-Doped Polymer Films to SLR-Supporting Arrays. The two boron dipyrromethene laser dyes used in these experiments as the energy donor, P580 (2,6-di-*n*-butyl-1,3,5,7,8 pentamethylpyrromethene-BF2, MW =

https://doi.org/10.1021/acsphotonics.1c00616
ACS Photonics 2021, 8, 2211−2219

374.32 g/mol), and acceptor, P650 (1,2,3,5,6,7-hexamethyl-8-cyanopyrromethene-BF2, MW = 301.15 g/mol), were both purchased from Luxottica-Exciton, and a 4 wt % solution of PMMA in anisole was purchased from Microchem (950 PMMA A4). The dyes were dissolved in the PMMA/anisole solution to make a mixed solution containing 27.0 mM P580 and 0.270 mM P650 along with 4 wt % PMMA in anisole. A total of 100 μL of this mixed solution was then spin-coated onto the Al-MIM lattices. Spinning was done at 4000 rpm for 60 s to achieve a 200 nm thick layer, as confirmed by stylus profilometry (Bruker Dektak-XT).

Optical Measurements. Confirmation and characterization of SLRs was done using angle-resolved spectroscopy. Specifically, angle-resolved spectra were collected using a Fourier microscope, like that described by Kurvits et al.,[63] except that this microscope included a Czerny-Turner monochromator. With the monochromator, the Fourier microscope setup becomes at Fourier spectroscope, in which one axis of the two-dimensional charge-coupled device corresponds to the k_x of the transmitted or emitted light, while the other axis corresponds to the wavelength. A diagram of this set up is shown in Figure S3 in the Supporting Information. For the measurement of transmission spectra, the side of the substrate with the Al-MIM nanocylinder lattices was covered with refractive index-matching oil (Cargille-type FF, n = 1.4811 at 546.1 nm) and a 170 μm thick glass coverslip. This was done so to make the environment around the Al-MIM lattices have an approximately uniform index of refraction ($n_2 \approx 1.48$), which is a precondition for obtaining the sharpest and clearest SLRs[2] and avoiding the splitting of each RA and SLR mode into a glass or substrate mode and an air or superstrate mode. For the measurement of angle-resolved transmission spectra of the lattices, the white light was focused on the Al-MIM lattices by a 100×, 0.6 numerical aperture (NA) objective (Olympus SLMPLN 100×, 0.6 NA, 7.6 mm working distance), and the transmitted light was collected by a 50×, 0.8 NA objective (Olympus MPLFLN 50×, 0.8 NA, 1 mm working distance). Later, the angle-resolved fluorescence spectra of the donor−PMMA and donor−acceptor−PMMA films were measured using only the 50×, 0.8 NA objective with a beam splitter for both excitation with the 488 nm pulsed laser and collection of the fluorescence emitted from the films, while the reflected laser light was removed with a 500 nm long-pass filter.

■ ASSOCIATED CONTENT

Supporting Information

The Supporting Information is available free of charge at https://pubs.acs.org/doi/10.1021/acsphotonics.1c00616.

(1) Computational model. (2) Experimental method. (3) Supplementary figures: Figure S1, theoretical extinction coefficient for different lattices; Figure S2, SLRs in different 1D NP arrays; Figure S3, diagram of Fourier microscope for measuring angle-resolved spectra; Figure S4, angle-integrated fluorescence spectra of 400 mM donor (P580) in PMMA on various SLR-supporting lattices. (4) Supplementary tables: Table S1, wavelengths of RAs and SLRs for Al-MIM nanocylinder lattices with various lattice constants; Table S2, FRET radius for P580 and P650 and predicted FRET efficiencies (η) for various dye concentrations; Table S3, approximations of the experimental FRET efficiencies; Table S4, percent change in FRET efficiency for the film on each lattice relative to the bare glass substrate; Table S5, comparisons of changes in I'_D to changes in I'_A for the four lattices (PDF)

■ AUTHOR INFORMATION

Corresponding Authors

Joel Yuen-Zhou − *Department of Chemistry and Biochemistry, University of California−San Diego, La Jolla, California 92093, United States*; Email: jyuenzhou@ucsd.edu

Vinod M. Menon − *Physics Department, The City College of New York, New York, New York 10031, United States; Department of Physics, Graduate Center, The Graduate Center of The City University of New York, New York, New York 10016, United States*; orcid.org/0000-0002-9725-6445; Email: vmenon@ccny.cuny.edu

Stephen O'Brien − *Ph.D. Program in Chemistry, The Graduate Center of the City University of New York, New York, New York 10016, United States; Department of Chemistry and Biochemistry, The City College of New York, New York, New York 10031, United States; The CUNY Energy Institute, The City College of New York, City University of New York, New York, New York 10031, United States*; orcid.org/0000-0001-7531-8900; Email: sobrien@ccny.cuny.edu

Authors

Robert Collison − *Ph.D. Program in Chemistry, The Graduate Center of the City University of New York, New York, New York 10016, United States; Department of Chemistry and Biochemistry, The City College of New York, New York, New York 10031, United States*; orcid.org/0000-0001-8895-9678

Juan B. Pérez-Sánchez − *Department of Chemistry and Biochemistry, University of California−San Diego, La Jolla, California 92093, United States*

Matthew Du − *Department of Chemistry and Biochemistry, University of California−San Diego, La Jolla, California 92093, United States*

Jacob Trevino − *Tandon School of Engineering, New York University, Brooklyn, New York 11201, United States*

Complete contact information is available at: https://pubs.acs.org/10.1021/acsphotonics.1c00616

Author Contributions

⊗Equal contribution by R.C. and J.B.P.-S.

Funding

R.C., V.M., and S.O. received funding from NSF Grant Number HRD-1547830 (CREST IDEALS). R.C. and S.O. received additional support from NSF DMR Award #1461499. J.B.P.S. and J.Y.Z. were supported by NSF EAGER CHE-1836599, while M.D. was supported by a UCSD Roger Tsien Fellowship.

Notes

The authors declare no competing financial interest.

■ ACKNOWLEDGMENTS

Fabrication and scanning electron microscopy were performed at the Advanced Science Research Center NanoFabrication Facility at the Graduate Center of the City University of New York (CUNY). Optical data was collected at the Laboratory for Nano- and Micro-Photonics (LaNMP), Department of

Physics, the City College of New York (CCNY). Thanks to Dr. Frederick Pearsall, Dr. Julien Lombardi, Nasim Farahmand, and Richard Hailin Huang, and also to Dr. Rahul Deshmukh, Dr. Nicholas Proscia, Mandeep Khatoniar, and the rest of the LaNMP team for technical guidance and fruitful discussions.

REFERENCES

(1) Auguié, B.; Barnes, W. L. Collective Resonances in Gold Nanoparticle Arrays. *Phys. Rev. Lett.* **2008**, *101* (14), 143902.
(2) Chu, Y.; Schonbrun, E.; Yang, T.; Crozier, K. B. Experimental Observation of Narrow Surface Plasmon Resonances in Gold Nanoparticle Arrays. *Appl. Phys. Lett.* **2008**, *93* (18), 181108.
(3) Guo, R.; Hakala, T. K.; Törmä, P. Geometry Dependence of Surface Lattice Resonances in Plasmonic Nanoparticle Arrays. *Phys. Rev. B: Condens. Matter Mater. Phys.* **2017**, *95* (15), 155423.
(4) Khlopin, D.; Laux, F.; Wardley, W. P.; Martin, J.; Wurtz, G. A.; Plain, J.; Bonod, N.; Zayats, A. V.; Dickson, W.; Gérard, D. Lattice Modes and Plasmonic Linewidth Engineering in Gold and Aluminum Nanoparticle Arrays. *J. Opt. Soc. Am. B* **2017**, *34* (3), 691−700.
(5) Knudson, M. P.; Li, R.; Wang, D.; Wang, W.; Schaller, R. D.; Odom, T. W. Polarization-Dependent Lasing Behavior from Low-Symmetry Nanocavity Arrays. *ACS Nano* **2019**, *13* (7), 7435−7441.
(6) Tretnak, V.; Hohenester, U.; Krenn, J. R.; Hohenau, A. The Role of Particle Size in the Dispersion Engineering of Plasmonic Arrays. *J. Phys. Chem. C* **2020**, *124* (3), 2104−2112.
(7) Zakharko, Y.; Rother, M.; Graf, A.; Hähnlein, B.; Brohmann, M.; Pezoldt, J.; Zaumseil, J. Radiative Pumping and Propagation of Plexcitons in Diffractive Plasmonic Crystals. *Nano Lett.* **2018**, *18* (8), 4927−4933.
(8) Hakala, T. K.; Moilanen, A. J.; Väkeväinen, A. I.; Guo, R.; Martikainen, J.-P.; Daskalakis, K. S.; Rekola, H. T.; Julku, A.; Törmä, P. Bose−Einstein Condensation in a Plasmonic Lattice. *Nat. Phys.* **2018**, *14* (7), 739−744.
(9) Yadav, R. K.; Otten, M.; Wang, W.; Cortes, C. L.; Gosztola, D. J.; Wiederrecht, G. P.; Gray, S. K.; Odom, T. W.; Basu, J. K. Strongly Coupled Exciton−Surface Lattice Resonances Engineer Long-Range Energy Propagation. *Nano Lett.* **2020**, *20* (7), 5043−5049.
(10) Lozano, G.; Louwers, D. J.; Rodríguez, S. R.; Murai, S.; Jansen, O. T.; Verschuuren, M. A.; Gómez Rivas, J. Plasmonics for Solid-State Lighting: Enhanced Excitation and Directional Emission of Highly Efficient Light Sources. *Light: Sci. Appl.* **2013**, *2* (5), No. e66.
(11) Yang, F.; Forrest, S. R. Photocurrent Generation in Nanostructured Organic Solar Cells. *ACS Nano* **2008**, *2* (5), 1022−1032.
(12) Penzo, E.; Loiudice, A.; Barnard, E. S.; Borys, N. J.; Jurow, M. J.; Lorenzon, M.; Rajzbaum, I.; Wong, E. K.; Liu, Y.; Schwartzberg, A. M.; Cabrini, S.; Whitelam, S.; Buonsanti, R.; Weber-Bargioni, A. Long-Range Exciton Diffusion in Two-Dimensional Assemblies of Cesium Lead Bromide Perovskite Nanocrystals. *ACS Nano* **2020**, *14* (6), 6999−7007.
(13) Knox, R. S. Förster's Resonance Excitation Transfer Theory: Not Just a Formula. *J. Biomed. Opt.* **2012**, *17* (1), No. 011003.
(14) Förster, T. Zwischenmolekulare Energiewanderung und Fluoreszenz. *Ann. Phys.* **1948**, *437* (1−2), 55−75.
(15) Feron, K.; Belcher, W. J.; Fell, C. J.; Dastoor, P. C. Organic Solar Cells: Understanding the Role of Förster Resonance Energy Transfer. *Int. J. Mol. Sci.* **2012**, *13* (12), 17019−17047.
(16) Feron, K.; Zhou, X.; Belcher, W. J.; Dastoor, P. C. Exciton Transport in Organic Semiconductors: Förster Resonance Energy Transfer Compared with a Simple Random Walk. *J. Appl. Phys.* **2012**, *111* (4), No. 044510.
(17) Lunt, R. R.; Giebink, N. C.; Belak, A. A.; Benziger, J. B.; Forrest, S. R. Exciton Diffusion Lengths of Organic Semiconductor Thin Films Measured by Spectrally Resolved Photoluminescence Quenching. *J. Appl. Phys.* **2009**, *105* (5), No. 053711.
(18) Deshmukh, R.; Biehs, S.-A.; Khwaja, E.; Galfsky, T.; Agarwal, G. S.; Menon, V. M. Long-Range Resonant Energy Transfer Using Optical Topological Transitions in Metamaterials. *ACS Photonics* **2018**, *5* (7), 2737−2741.
(19) Zhong, X.; Chervy, T.; Wang, S.; George, J.; Thomas, A.; Hutchison, J. A.; Devaux, E.; Genet, C.; Ebbesen, T. W. Non-Radiative Energy Transfer Mediated by Hybrid Light-Matter States. *Angew. Chem., Int. Ed.* **2016**, *55* (21), 6202−6206.
(20) Zhong, X.; Chervy, T.; Zhang, L.; Thomas, A.; George, J.; Genet, C.; Hutchison, J. A.; Ebbesen, T. W. Energy Transfer between Spatially Separated Entangled Molecules. *Angew. Chem., Int. Ed.* **2017**, *56* (31), 9034−9038.
(21) Coles, D. M.; Somaschi, N.; Michetti, P.; Clark, C.; Lagoudakis, P. G.; Savvidis, P. G.; Lidzey, D. G. Polariton-Mediated Energy Transfer between Organic Dyes in a Strongly Coupled Optical Microcavity. *Nat. Mater.* **2014**, *13* (7), 712−719.
(22) Georgiou, K.; Michetti, P.; Gai, L.; Cavazzini, M.; Shen, Z.; Lidzey, D. G. Control over Energy Transfer between Fluorescent BODIPY Dyes in a Strongly Coupled Microcavity. *ACS Photonics* **2018**, *5* (1), 258−266.
(23) Lunz, M.; Gerard, V. A.; Gun'ko, Y. K.; Lesnyak, V.; Gaponik, N.; Susha, A. S.; Rogach, A. L.; Bradley, A. L. Surface Plasmon Enhanced Energy Transfer between Donor and Acceptor CdTe Nanocrystal Quantum Dot Monolayers. *Nano Lett.* **2011**, *11* (8), 3341−3345.
(24) Andrew, P.; Barnes, W. L. Energy Transfer Across a Metal Film Mediated by Surface Plasmon Polaritons. *Science* **2004**, *306* (5698), 1002−1005.
(25) Du, M.; Martinez-Martinez, L. A.; Ribeiro, R. F.; Hu, Z.; Menon, V. M.; Yuen-Zhou, J. Theory for Polariton-Assisted Remote Energy Transfer. *Chem. Sci.* **2018**, *9* (32), 6659−6669.
(26) Baibakov, M.; Patra, S.; Claude, J.-B.; Moreau, A.; Lumeau, J.; Wenger, J. Extending Single-Molecule Förster Resonance Energy Transfer (FRET) Range beyond 10 Nanometers in Zero-Mode Waveguides. *ACS Nano* **2019**, *13* (7), 8469−8480.
(27) Purcell, E. M.; Torrey, H. C.; Pound, R. V. Resonance Absorption by Nuclear Magnetic Moments in a Solid. *Phys. Rev.* **1946**, *69* (1−2), 37−38.
(28) Purcell, E. M. Spontaneous Emission Probabilities at Radio Frequencies. *Phys. Rev.* **1946**, *69* (11−12), 674−674.
(29) Andrew, P.; Barnes, W. L. Förster Energy Transfer in an Optical Microcavity. *Science* **2000**, *290* (5492), 785−788.
(30) Hamza, A. O.; Viscomi, F. N.; Bouillard, J.-S. G.; Adawi, A. M. Förster Resonance Energy Transfer and the Local Optical Density of States in Plasmonic Nanogaps. *J. Phys. Chem. Lett.* **2021**, *12* (5), 1507−1513.
(31) Konrad, A.; Metzger, M.; Kern, A. M.; Brecht, M.; Meixner, A. J. Controlling the Dynamics of Förster Resonance Energy Transfer inside a Tunable Sub-Wavelength Fabry−Pérot-Resonator. *Nanoscale* **2015**, *7* (22), 10204−10209.
(32) Blum, C.; Zijlstra, N.; Lagendijk, A.; Wubs, M.; Mosk, A. P.; Subramaniam, V.; Vos, W. L. Nanophotonic Control of the Förster Resonance Energy Transfer Efficiency. *Phys. Rev. Lett.* **2012**, *109* (20), 203601.
(33) Wubs, M.; Vos, W. L. Foerster Resonance Energy Transfer Rate and Local Density of Optical States Are Uncorrelated in Any Dielectric Nanophotonic Medium. *New J. Phys.* **2016**, *18*, 053037.
(34) Wubs, M.; Vos, W. L. Förster Resonance Energy Transfer Rate in Any Dielectric Nanophotonic Medium with Weak Dispersion. *New J. Phys.* **2016**, *18* (5), No. 053037.
(35) Knight, M. W.; King, N. S.; Liu, L.; Everitt, H. O.; Nordlander, P.; Halas, N. J. Aluminum for Plasmonics. *ACS Nano* **2014**, *8* (1), 834−840.
(36) Olson, J.; Manjavacas, A.; Liu, L.; Chang, W.-S.; Foerster, B.; King, N. S.; Knight, M. W.; Nordlander, P.; Halas, N. J.; Link, S. Vivid, Full-Color Aluminum Plasmonic Pixels. *Proc. Natl. Acad. Sci. U. S. A.* **2014**, *111* (40), 14348−14353.
(37) Tan, S. J.; Zhang, L.; Zhu, D.; Goh, X. M.; Wang, Y. M.; Kumar, K.; Qiu, C.-W.; Yang, J. K. W. Plasmonic Color Palettes for Photorealistic Printing with Aluminum Nanostructures. *Nano Lett.* **2014**, *14* (7), 4023−4029.

https://doi.org/10.1021/acsphotonics.1c00616
ACS Photonics 2021, 8, 2211−2219

(38) Eizner, E.; Avayu, O.; Ditcovski, R.; Ellenbogen, T. Aluminum Nanoantenna Complexes for Strong Coupling between Excitons and Localized Surface Plasmons. *Nano Lett.* **2015**, *15* (9), 6215−6221.
(39) Todisco, F.; Esposito, M.; Panaro, S.; De Giorgi, M.; Dominici, L.; Ballarini, D.; Fernández-Domínguez, A. I.; Tasco, V.; Cuscunà, M.; Passaseo, A.; Ciracì, C.; Gigli, G.; Sanvitto, D. Toward Cavity Quantum Electrodynamics with Hybrid Photon Gap-Plasmon States. *ACS Nano* **2016**, *10* (12), 11360−11368.
(40) Chow, C.; Bain, J. A. Effect of Thin Cr and Cu Adhesion Layers on Surface Plasmon Resonance at Au/SiO2 Interfaces. *IEEE Trans. Magn.* **2016**, *52* (7), 1−4.
(41) Debu, D. T.; Ghosh, P. K.; French, D.; Herzog, J. B. Surface Plasmon Damping Effects Due to Ti Adhesion Layer in Individual Gold Nanodisks. *Opt. Mater. Express* **2017**, *7* (1), 73−84.
(42) Habteyes, T. G.; Dhuey, S.; Wood, E.; Gargas, D.; Cabrini, S.; Schuck, P. J.; Alivisatos, A. P.; Leone, S. R. Metallic Adhesion Layer Induced Plasmon Damping and Molecular Linker as a Nondamping Alternative. *ACS Nano* **2012**, *6* (6), 5702−5709.
(43) Siegfried, T.; Ekinci, Y.; Martin, O. J. F.; Sigg, H. Engineering Metal Adhesion Layers That Do Not Deteriorate Plasmon Resonances. *ACS Nano* **2013**, *7* (3), 2751−2757.
(44) Wang, H.; Wang, X.; Yan, C.; Zhao, H.; Zhang, J.; Santschi, C.; Martin, O. J. F. Full Color Generation Using Silver Tandem Nanodisks. *ACS Nano* **2017**, *11* (5), 4419−4427.
(45) Yu, A.; Li, W.; Wang, Y.; Li, T. Surface Lattice Resonances Based on Parallel Coupling in Metal-Insulator-Metal Stacks. *Opt. Express* **2018**, *26* (16), 20695−20707.
(46) Yang, X.; Xiao, G.; Lu, Y.; Li, G. Narrow Plasmonic Surface Lattice Resonances with Preference to Asymmetric Dielectric Environment. *Opt. Express* **2019**, *27* (18), 25384−25394.
(47) Deeb, C.; Guo, Z.; Yang, A.; Huang, L.; Odom, T. W. Correlating Nanoscopic Energy Transfer and Far-Field Emission to Unravel Lasing Dynamics in Plasmonic Nanocavity Arrays. *Nano Lett.* **2018**, *18* (2), 1454−1459.
(48) Shi, L.; Hakala, T. K.; Rekola, H. T.; Martikainen, J.-P.; Moerland, R. J.; Törmä, P. Spatial Coherence Properties of Organic Molecules Coupled to Plasmonic Surface Lattice Resonances in the Weak and Strong Coupling Regimes. *Phys. Rev. Lett.* **2014**, *112* (15), 153002.
(49) Yadav, R. K.; Bourgeois, M. R.; Cherqui, C.; Juarez, X. G.; Wang, W.; Odom, T. W.; Schatz, G. C.; Basu, J. K. Room Temperature Weak-to-Strong Coupling and the Emergence of Collective Emission from Quantum Dots Coupled to Plasmonic Arrays. *ACS Nano* **2020**, *14* (6), 7347−7357.
(50) Cherqui, C.; Bourgeois, M. R.; Wang, D.; Schatz, G. C. Plasmonic Surface Lattice Resonances: Theory and Computation. *Acc. Chem. Res.* **2019**, *52* (9), 2548−2558.
(51) Anger, P.; Bharadwaj, P.; Novotny, L. Enhancement and Quenching of Single-Molecule Fluorescence. *Phys. Rev. Lett.* **2006**, *96* (11), 113002.
(52) Cortes, C. L.; Jacob, Z. Fundamental Figures of Merit for Engineering Förster Resonance Energy Transfer. *Opt. Express* **2018**, *26* (15), 19371−19387.
(53) Huang, J.-S.; Goh, T.; Li, X.; Sfeir, M. Y.; Bielinski, E. A.; Tomasulo, S.; Lee, M. L.; Hazari, N.; Taylor, A. D. Polymer Bulk Heterojunction Solar Cells Employing Förster Resonance Energy Transfer. *Nat. Photonics* **2013**, *7* (6), 479−485.
(54) Goh, T.; Huang, J.-S.; Yager, K. G.; Sfeir, M. Y.; Nam, C.-Y.; Tong, X.; Guard, L. M.; Melvin, P. R.; Antonio, F.; Bartolome, B. G.; Lee, M. L.; Hazari, N.; Taylor, A. D. Solar Cells: Quaternary Organic Solar Cells Enhanced by Cocrystalline Squaraines with Power Conversion Efficiencies >10%. *Adv. Energy Mater.* **2016**, *6* (21), na.
(55) Kong, J.; Mohadjer Beromi, M.; Mariano, M.; Goh, T.; Antonio, F.; Hazari, N.; Taylor, A. D. Colorful Polymer Solar Cells Employing an Energy Transfer Dye Molecule. *Nano Energy* **2017**, *38*, 36−42.
(56) Feron, K.; Cave, J. M.; Thameel, M. N.; O'Sullivan, C.; Kroon, R.; Andersson, M. R.; Zhou, X.; Fell, C. J.; Belcher, W. J.; Walker, A. B.; Dastoor, P. C. Utilizing Energy Transfer in Binary and Ternary Bulk Heterojunction Organic Solar Cells. *ACS Appl. Mater. Interfaces* **2016**, *8* (32), 20928−20937.
(57) Cnops, K.; Rand, B. P.; Cheyns, D.; Verreet, B.; Empl, M. A.; Heremans, P. 8.4% Efficient Fullerene-Free Organic Solar Cells Exploiting Long-Range Exciton Energy Transfer. *Nat. Commun.* **2014**, *5* (1), 1−6.
(58) Ziessel, R.; Ulrich, G.; Haefele, A.; Harriman, A. An Artificial Light-Harvesting Array Constructed from Multiple Bodipy Dyes. *J. Am. Chem. Soc.* **2013**, *135* (30), 11330−11344.
(59) Baldo, M. A.; Thompson, M. E.; Forrest, S. R. High-Efficiency Fluorescent Organic Light-Emitting Devices Using a Phosphorescent Sensitizer. *Nature* **2000**, *403* (6771), 750−753.
(60) Nabiev, I.; Rakovich, A.; Sukhanova, A.; Lukashev, E.; Zagidullin, V.; Pachenko, V.; Rakovich, Y. P.; Donegan, J. F.; Rubin, A. B.; Govorov, A. O. Fluorescent Quantum Dots as Artificial Antennas for Enhanced Light Harvesting and Energy Transfer to Photosynthetic Reaction Centers. *Angew. Chem., Int. Ed.* **2010**, *49* (40), 7217−7221.
(61) Wang, D.; Bourgeois, M. R.; Lee, W.-K.; Li, R.; Trivedi, D.; Knudson, M. P.; Wang, W.; Schatz, G. C.; Odom, T. W. Stretchable Nanolasing from Hybrid Quadrupole Plasmons. *Nano Lett.* **2018**, *18* (7), 4549−4555.
(62) Yang, A.; Hoang, T. B.; Dridi, M.; Deeb, C.; Mikkelsen, M. H.; Schatz, G. C.; Odom, T. W. Real-Time Tunable Lasing from Plasmonic Nanocavity Arrays. *Nat. Commun.* **2015**, *6*, 6939.
(63) Kurvits, J. A.; Jiang, M.; Zia, R. Comparative Analysis of Imaging Configurations and Objectives for Fourier Microscopy. *J. Opt. Soc. Am. A* **2015**, *32* (11), 2082−2092.

https://doi.org/10.1021/acsphotonics.1c00616
ACS Photonics 2021, 8, 2211−2219